JOURNAL OF SPACECRAFT AND ROCKETS
Vol. 33, No. 5, September–October 1996

Microgravity Experiment Acceleration Tolerability on Space Orbiting Laboratories

R. Monti* and R. Savino†
University of Naples "Federico II," Naples 80125, Italy

Residual gravity and *g* jitter aboard space orbiting laboratories induce disturbing effects on fluid and material science experiments. A nondimensional scaling analysis of the field equations, under the assumption of high frequencies and small amplitudes of *g* jitter, was carried out to assess the tolerability criteria for microgravity experiments in the presence of oscillatory and time-averaged fluid thermodynamic distortions induced by multiple-frequency excitation. The most important result is that the tolerability limits, imposed by the presence of time-averaged distortions, are substantially lower than those corresponding to oscillatory distortions. The tolerability domains, in the plane of frequency vs acceleration, were numerically computed for a specific test case consisting of a directional solidification process of binary alloys or semiconductors.

Nomenclature

b = amplitude of the sinusoidal displacement, cm
c = mass concentration measured with respect to its reference value
c_s = solute concentration at the crystal–melt interface in a solid
c_0 = solute concentration at the crystal–melt interface in a fluid
c_∞ = solute concentration of the feed material
D = mass diffusion coefficient, cm^2/s
G = amplitude of g disturbance scaled by the Earth-gravity acceleration
G_s = residual g level scaled by the Earth-gravity acceleration
g = acceleration of gravity, cm/s^2
g_s = steady residual g level, cm/s^2
g_0 = Earth-gravity acceleration, 980 cm/s^2
H = vertical length (along y axis), cm
k = segregation coefficient
L = horizontal length (along x axis), cm
l = scale factor in direction of the prevailing diffusion term
$\boldsymbol{n}$ = unit vector of the vibration axis
Pe_c = solute Peclet number defined in terms of the growth velocity ($V_c L/D$)
Pe_g = gravitational Peclet number
Pe_v = vibrational Peclet number
Pr = Prandtl number (ν/α)
p = pressure, dyne/cm^2
Re_g = Reynolds number defined in terms of the gravitational speed ($V_g L/\nu$)
$\boldsymbol{r}$ = position vector at the boundary, cm
Sc = Schmidt number, ν/D
Sr_v = Strouhal number defined in terms of the viscous diffusion time ($\omega L^2/\nu$)
T = temperature measured with respect to its reference value, K
t = time, s
u, v = normalized velocity components along x, y directions
$\boldsymbol{V}$ = flow velocity, cm/s
V_c = crystal growth velocity, cm/s
V_g = gravitational velocity, cm/s
V_v = vibrational velocity, cm/s
$\boldsymbol{w}$ = solenoidal part of $(\beta_T T + \beta_c c)\, n$
x, y = normalized Cartesian coordinates
α = thermal diffusivity, cm^2/s
β_c = solute expansion coefficient
β_T = thermal expansion coefficient, K^{-1}
Δc = imposed concentration difference
ΔT = imposed temperature difference, K
Δ_2 = Laplacian operator
$\varepsilon_{\text{long}}$ = longitudinal concentration distortion
ε_{rad} = radial concentration distortion
μ = dynamic viscosity, g cm^{-1} s^{-1}
ν = kinematic viscosity, cm^2/s
ρ = fluid density, g/cm^3
σ = ratio of melt and crystal densities
ω = angular velocity of the sinusoidal g disturbance, s^{-1}
ω_v = viscous diffusion frequency, s^{-1}

Subscripts

r = reference
t = partial derivation with respect to time
max = maximum allowable value

Introduction

SYSTEMATIC characterization of the acceleration aboard space platforms has shown that microgravity is a dynamic environment resulting from many sources, e.g., gravity gradient and aerodynamic forces, solar pressure, attitude-control actuation, onboard machinery, crew operations, servicing activities, docking/berthing.[1–3] Steady or quasisteady forces are responsible for residual-gravity levels. Other time-dependent forces (impulsive, periodic) are responsible for g jitter. Distortions of the thermal and concentration fields may be caused by the convection associated with steady residual-gravity levels, with g jitter, or with both.

The principal investigator needs information on the actual gravitational environment encountered in spaceflights, on its predicted effect on the experiment and, in postflight analysis, on how to correlate his or her predictions with the actual results obtained. The investigator would like to select the microgravity platform that is most appropriate for hosting the experiment, on the basis of the time profile of the actual acceleration field. Space agencies, manufacturers of flight experiment hardware, and designers of spaceflight systems, on the other hand, need to guarantee an appropriate envelope of microgravity conditions onboard the platform. Therefore, specifications must be given for the maximum gravitational disturbances that may be generated by different facilities and by crew activities.

Received Aug. 14, 1995; revision received Feb. 23, 1996; accepted for publication March 15, 1996.

*Full Professor of Aerodynamics, Department of Space Science and Engineering "L.G. Napolitano," P. le V. Tecchio 80.

†Researcher, Department of Space Science and Engineering "L.G. Napolitano," P. le V. Tecchio 80.

The activities performed up to now have been mainly devoted to the prediction of the tolerability limits following scaling-analysis techniques.[4,5] Numerical studies have been developed to evaluate the effects of residual accelerations in enclosures[6] or time-dependent acceleration fields that are either periodic in time or a sequence of isolated pulses of short duration.[7–9]

There also are a number of numerical analyses of space experiments available.[10–12] As shown theoretically and experimentally in the Russian literature, however, vibrations in the presence of temperature or concentration gradients can give rise to nonzero-average steady motion superimposed on a zero-average periodic flow (thermal or solute vibrational convection[13,14]). If this new mechanism of convection is taken into account, a new tolerability analysis is to be performed to evaluate more accurate maximum allowable g levels of high-frequency periodic disturbances.

A new tolerability criterion to assess the maximum allowable g level at high frequency is formulated, on the basis of an order-of-magnitude analysis of the time-averaged field equations, either for thermally driven natural convection or for solute-driven natural convection in a nonisothermal binary mixture, in the presence of residual gravity and multiple-frequency excitation. This analysis allows one to estimate the temperature or the concentration distortions caused by the convection associated with temperature or concentration differences. A general fluid-dynamics code has been developed to evaluate the thermal and concentration distortions. As a challenging example, the tolerability limits for directional solidification of typical binary alloys and semiconductors are evaluated, for which the distortion of the concentration field is caused by the cross effect of thermal buoyancy-driven convection.

Modeling Required for the g Tolerability Definition

The tolerability of an experiment to acceleration disturbances includes (Fig. 1) a) the process involved; b) the expected results in a reference situation (reference product, e.g., the product obtainable in the ideal zero-gravity environment); c) the types of g disturbances present in the environment; and d) the tolerable difference between the microgravity and the reference product.

The thermo-fluid-dynamic (TFD) distortions are defined as the differences between the actual TFD fields and those prevailing in zero gravity or in reference conditions. These distortions are responsible for the differences between the zero-gravity (or the reference) and the actual product of the space processing. The reference product may be taken to be either that corresponding to zero gravity (ideal conditions) or that obtainable on the platform subjected to residual gravity levels only.

If accurate TFD and process models were available, then it would be possible to evaluate the effects of different background residual accelerations and various transient disturbances on the final products, to check that the expected microgravity environment offered by the different platforms is suitable for the selected space processing, and to identify the tolerability limits for different types of g jitter superimposed on the steady residual-gravity-levels.

The TFD modeling is general (general classes of fluid-dynamics problems can be studied), whereas the process modeling requires more specific formulations (e.g., appropriate equations and boundary conditions for crystal growth, solidification, or other material science processes). Because the process models are usually very complex, we can evaluate the TFD distortions by sophisticated TFD modeling and assume that the products are proportional to the causes far away from stability limits.

This can be assessed by means of an order-of-magnitude analysis or via specific numerical models.

In an order-of-magnitude analysis, the various terms in the governing equations are estimated by use of appropriate scales characteristic of the ranges of variation of the relevant physical parameters. This allows one to derive relations, often in the form of simple laws, between the relevant nondimensional parameters of the process. Because of the approximate nature of such an analysis, it always should be performed in parallel with either numerical simulations or experiments to guarantee the validity of the model. After validation, however, the results can be handled easily by the practitioner because the algebra involved is quite simple. Scaling and order-of-magnitude analyses thus may always be used to perform an a priori check on the microgravity relevance of a given fluid and material science experiment.

Basic Assumptions and Field Equations

We assume that the fluid system is subjected to a number of stimuli (imposed temperature and/or concentration differences), as well as to the gravitational forces representing the disturbances from the zero-gravity condition. The fluid is supposed to be homogeneous and Newtonian, with constant transport coefficients; the Boussinesq approximation applies for density; viscous energy dissipation is negligible.

Under the above hypotheses, the flow is governed by the continuity, Navier–Stokes, energy, and solute mass equations:

$$\nabla \cdot V = 0 \tag{1a}$$

$$V_t + V \cdot \nabla V + (1/\rho_r)\nabla p = \nu \Delta_2 V + [(\rho - \rho_r)/\rho_r]\boldsymbol{g}(t) \tag{1b}$$

$$T_t + V \cdot \nabla T = \alpha \Delta_2 T \tag{1c}$$

$$c_t + V \cdot \nabla c = D \Delta_2 c \tag{1d}$$

The density is assumed to be a linear function of the temperature and of the concentration, measured with respect to their reference values:

$$\rho = \rho_r(1 - \beta_T T - \beta_c c) \tag{2}$$

At the fluid cell boundaries, if a sinusoidal motion is applied, the position vector $\boldsymbol{r}$ on the boundary is a sinusoidal function of time:

$$\boldsymbol{r}(t) = b\cos(\omega t)\boldsymbol{n} \tag{3a}$$

This gives rise to a velocity and acceleration:

$$V(t) = -b\omega \sin(\omega t)\boldsymbol{n} \tag{3b}$$

$$\boldsymbol{g}_\omega(t) = -b\omega^2 \cos(\omega t)\boldsymbol{n} \tag{3c}$$

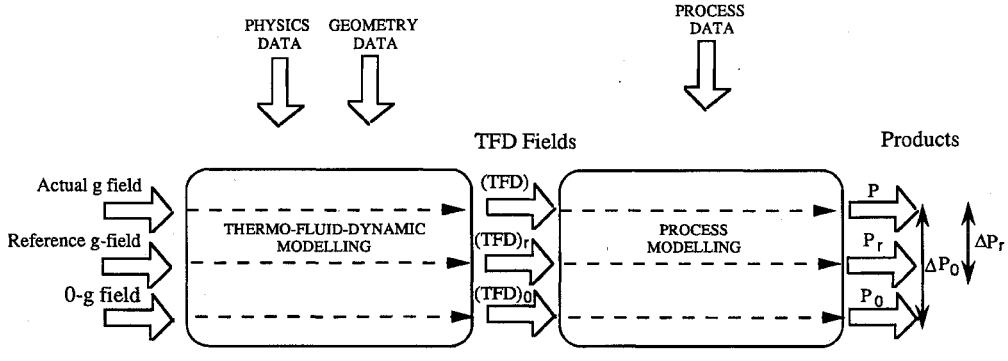

Fig. 1 Schematics of the modeling required for the g tolerability definition.

In general, a number of high-frequency periodic vibrations (g jitter) of different amplitudes, frequencies, and direction are applied, and a residual (steady) acceleration field can be superposed, so that the overall body force is

$$\boldsymbol{g}(t) = \boldsymbol{g}_s - \sum_{i=1}^{m} b_i \omega_i^2 \cos(\omega_i t)\boldsymbol{n}_i \tag{4}$$

Time-Averaged Formulation

Under the assumptions that the vibration period is much less than the characteristic energy and mass diffusion times and that the amplitude of the oscillation is very small, each TFD variable can be separated into a pulsating component (with frequency ω) and a time-averaged part (over times much larger than ω^{-1}).

For the pulsating flow, the momentum equation is obtained, retaining only the time-dependent term, the pressure term, and the linearized driving term (convective and diffusive terms are negligible, as shown by an appropriate order-of-magnitude analysis[15]):

$$\boldsymbol{V}'t + \frac{1}{\rho_r}\nabla p' = \sum_{i=1}^{m} b_i \omega_i^2 (\beta_T T + \beta_c c)\cos(\omega_i t)\boldsymbol{n} \tag{5a}$$

The equations for the temperature and concentration fluctuation read as follows:

$$T_t' + \boldsymbol{V}' \cdot \nabla T = 0 \tag{5b}$$

$$c_t' + \boldsymbol{V}' \cdot \nabla c = 0 \tag{5c}$$

If the vector $(\beta_T T + \beta_c c)\boldsymbol{n}$ is expressed as

$$(\beta_T T + \beta_c c)\boldsymbol{n} = \boldsymbol{w} + \nabla\varphi \tag{6a}$$

with

$$\nabla \cdot \boldsymbol{w} = 0 \tag{6b}$$

$$\nabla \wedge \boldsymbol{w} = \nabla(\beta_T T + \beta_c c) \wedge \boldsymbol{n} \tag{6c}$$

the equation for the pulsating velocity can be separated into two equations (for the potential and the solenoidal parts):

$$\boldsymbol{V}'t = \sum_{i=1}^{m} b_i \omega_i^2 \boldsymbol{w} \cos(\omega_i t) \tag{7a}$$

$$\frac{1}{\rho_r}\nabla p' = \sum_{i=1}^{m} b_i \omega_i^2 \nabla\varphi \cos(\omega_i t) \tag{7b}$$

Integration with respect to time of Eq. (7a) yields

$$\boldsymbol{V}' = \sum_{i=1}^{m} b_i \omega_i \boldsymbol{w} \sin(\omega_i t) \tag{7c}$$

which, substituted into Eqs. (5b) and (5c), gives

$$T' = -\sum_{i=1}^{m} b_i \cos(\omega_i t)\boldsymbol{w} \cdot \nabla T \tag{8a}$$

$$c' = -\sum_{i=1}^{m} b_i \cos(\omega_i t)\boldsymbol{w} \cdot \nabla c \tag{8b}$$

Use of Eqs. (7c), (8a), and (8b) and evaluation of the averaged values lead to the following final system, in the general case of a dilute binary mixture subjected to a body force including a residual-gravity vector and a number of high-frequency sinusoidal disturbances:

$$\nabla \cdot \boldsymbol{V} = 0 \tag{9a}$$

$$\boldsymbol{V}_t + \boldsymbol{V} \cdot \nabla\boldsymbol{V} + \frac{1}{\rho_r}\nabla p = \nu\Delta_2 \boldsymbol{V} - (\beta_T T + \beta_c c)\boldsymbol{g}_s + \left[\sum_{i=1}^{m} \frac{1}{2}(b_i\omega_i)^2\right][\boldsymbol{w} \cdot \nabla(\beta_T T + \beta_c c)\boldsymbol{n} - \boldsymbol{w} \cdot \nabla\boldsymbol{w}] \tag{9b}$$

$$T_t + \boldsymbol{V} \cdot \nabla T = \alpha\Delta_2 T \tag{9c}$$

$$c_t + \boldsymbol{V} \cdot \nabla c = D\Delta_2 c \tag{9d}$$

$$\nabla \cdot \boldsymbol{w} = 0 \tag{9e}$$

$$\nabla \wedge \boldsymbol{w} = \nabla(\beta_T T + \beta_c c) \wedge \boldsymbol{n} \tag{9f}$$

A scaling and order-of-magnitude analysis of the problem is performed in the next paragraph, and then, numerical solutions of the equations are discussed, with reference to the study case mentioned in the Introduction.

Scaling Analysis of Microgravity Tolerability Criteria

If only oscillatory effects are taken into account in the momentum Eq. (1b), measuring all terms with respect to the driving action, the nondimensional coefficients read as follows:

$$1$$
(driving g term)

$$\frac{V_r}{V_g l^2}$$
(diffusive term)

$$\frac{V_r^2 L_r}{\nu V_g}$$
(convective term)

$$\frac{\omega L_r^2 f}{\nu}\frac{V_r}{V_g}$$
(unsteady term)

where V_g is the characteristic buoyant velocity, given by

$$V_g = \frac{g\Delta\rho L_r^2}{\mu} \tag{10}$$

and $\Delta\rho = \rho_r \beta_T \Delta T$ for the case of thermal convection and $\Delta\rho = \rho_r \beta_c \Delta c$ for solute convection.

For quasisteady residual gravity ($\omega \to 0$), the unsteady term is negligible, and the diffusive term must balance the driving one ($V_r = V_g l^2$). Because no boundary layers are present, $l = 1$ and $V_r = V_g$.

For high-frequency single-sinusoidal disturbances ($\omega \to \infty$), the unsteady term prevails and balances the driving one ($V_r = V_g \nu/\omega L_r^2$). In this case, the convective term is negligible, and the scale factor is determined by the condition that the measure of the diffusive term with respect to the driving action be, at most, of order of magnitude one.

Typically, one is interested in how the zero-gravity (diffusion-controlled) temperature (or concentration) fields are distorted by the convective flows induced by the residual acceleration field prevailing on microgravity platforms. The order of magnitude of the thermal (or solute) distortions depends on the relative importance of the convective terms in the transport equations (energy or mass species equation).

In the case of quasisteady residual gravity ($\omega \to 0$; $V_r = V_g$), we have

$$V_r L_r/\eta = V_g L_r/\eta = Pe_g \tag{11}$$

where $\eta = \alpha$ for the energy equation and $\eta = D$ for the solute species equation.

In the case of high-frequency g jitter,

$$(V_r L_r/\eta) l^2 = Pe_g/Sr_v^2 \tag{12}$$

For the definition of the tolerability criteria, we must impose that the relative importance of convective and diffusive terms is less than or equal to a prescribed maximum allowed value.

After these assumptions and specifications, the maximum g level for the two cases of quasisteady residual gravity and sinusoidal disturbances at relatively high frequency is obtained as a function of the maximum allowable Peclet number:

Quasisteady residual gravity ($\omega L_r^2/\nu \ll 1$)

$$G_{\max} = \left(\frac{g}{g_0}\right)_{\max} = (Pe_g)_{\max} \frac{\rho \nu \eta}{g_0 \Delta\rho L_r^3} \tag{13a}$$

Single-frequency g jitter ($\omega L_r^2/\nu \gg 1$)

$$G_{\max} = \left(\frac{g}{g_0}\right)_{\max} = \left(Pe_g l^2\right)_{\max} \frac{\rho \eta L_r}{g_0 \nu \Delta\rho} \omega^2 \tag{13b}$$

If average vibrational effects are taken into account, from the scaling analysis of the momentum Eq. (9b), one finds that the reference velocity characteristic of the vibrational convection is

$$V_v = \frac{(b\omega\Delta\rho)^2 L_r}{2\rho^2 \nu} \tag{14}$$

The measure of the convective to the diffusive term in the transport equations (i.e., the disturbance induced by convection in an otherwise diffusion-controlled process taking place in a quiescent medium) is given by the vibrational Peclet number:

$$Pe_v = \frac{V_r L_r}{\eta} = \frac{(b\omega\Delta\rho)^2 L_r^2}{2\rho^2 \nu \eta} \tag{15}$$

The g level inducing the maximum allowable average distortion is obtained as a function of the maximum allowable vibrational Peclet number:

$$G_{\max} = \omega \sqrt{Pe_{v_{\max}}} \frac{\rho\sqrt{2\nu\eta}}{g_0 \Delta\rho L_r} \tag{16}$$

Equations (13a), (13b), and (16) identify the functional dependence of $G_{\max}$ on the fluid properties, on the maximum allowable Peclet number, and on the frequency, i.e., the different tolerability domains, as measured by acceleration as a function of frequency. Obviously, the reference scale length is related to the geometric length, and its correct value depends on the particular application. Therefore, Eqs. (13a), (13b), and (16) can be used in an order-of-magnitude analysis to identify the tolerability domains for different classes of experiments if an appropriate value of the reference-length scale (depending on the particular problem) is introduced, and a maximum value of the Peclet number is prescribed as a measure of the maximum tolerable field distortion; or, if computational models are available and a correlation law between the Peclet number and a suitable defined distortion parameter is obtained, the maximum allowable g levels are determined, in correspondence of the maximum allowable value of the distortion parameter, by introducing, in Eqs. (13a), (13b), and (16), the corresponding computed value of the Peclet number (a specific example is carried out in the next section, for a Bridgman crystal-growth process). A plot of the different tolerability domains is illustrated in Fig. 2. In the range of low frequency (quasisteady g disturbances), a straight line corresponding to constant maximum g level represents the tolerability limit associated with conventional natural convection. The distortions induced by high-frequency acceleration are divided into two categories: oscillatory and time-averaged TFD disturbances. The tolerability limits attributable to oscillatory distortions correspond to a quadratic dependence of the tolerable g level on the frequency. By contrast, the limits corresponding to time-averaged distortions

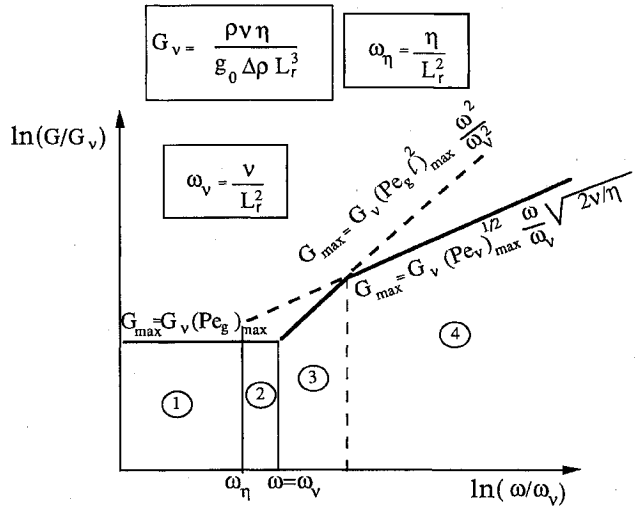

Fig. 2 Tolerability limits in the plane frequency, acceleration: ①, purely diffusive (governed by steady g); ②, for $Pr < 1$, still governed by steady g; ③, tolerance defined by oscillatory effects; and ④, tolerance defined by time-averaged effects.

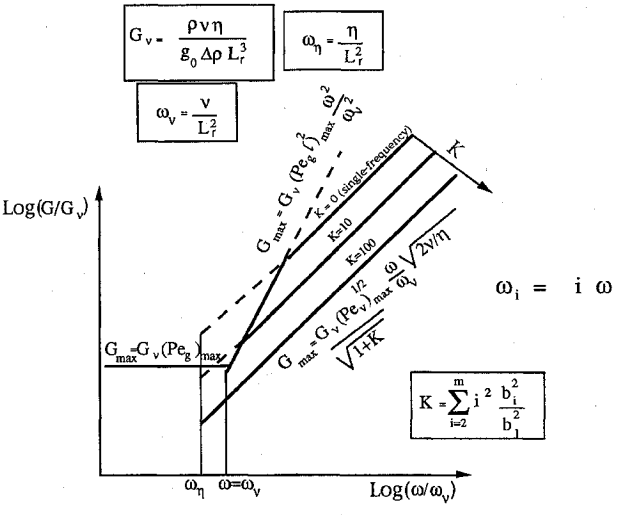

Fig. 3 Tolerability domains for multiple-frequency excitation; ω = fundamental frequency.

follow a linear dependence. Moreover, the oscillatory g limits apply only to single-frequency disturbances and, on the contrary, the averaged g limits may account for practically any number of frequencies simultaneously acting on the experiment cell. In fact, from Eq. (9b) the average thermal and solute distortions do not depend separately on the amplitudes and on the frequencies of the various disturbances, but are only functions of the equivalent vibrational Peclet number:

$$Pe_v = \sum_{i=1}^{m} Pe_{vi} \tag{17}$$

This implies that the tolerability criterion can be generalized easily to the case of multiple-frequency excitation in terms of the equivalent vibrational Peclet number.

In Fig. 3, the tolerability domains are extended to the general case by introducing a parameter

$$K = \sum_{i=2}^{m} i^2 b_i^2 / b_1^2$$

accounting for the presence of more periodic disturbances. The allowable g level corresponding to multiple-frequency excitation is determined by entering the diagram at the fundamental frequency

and assuming that the tolerability limit is given by the straight line characterized by the appropriate value of K. The situation of single-frequency disturbance is recovered, as in the particular case, for $K = 0$.

From the measurements performed and from the theoretical predictions obtained for different microgravity platforms, it follows that the amplitude G of oscillatory disturbances is roughly a linear function of the frequency ω, so that for a given platform, the term $b^2\omega^2$ appearing in the definition of the vibrational Peclet number should be of the same order of magnitude for the different disturbances associated with the different sources of g jitter (e.g., different machineries or crew activities).

Numerical Solutions for Bridgman Crystal Growth

The physical situation under investigation and the idealized model are shown in Fig. 4. We consider a horizontal ampoule containing a dilute two-component melt. Directional solidification takes place as the ampoule is translated through fixed hot and cold zones. With reference to Fig. 1, in this case the TFD model allows one to compute radial or longitudinal distortions of the concentration profiles in the melt, but it is difficult to relate these distortions to the final quality of the solid crystals. For a crystal growing with a plane interface, the crystal will have a composition given by the product of the segregation coefficient and the composition on the melt at the growth interface; this determines radial segregation. The distortions of the composition in the melt away from the growth interface, which affects the average composition at the interface, determine axial segregation. However, even if these phenomena were taken into account, it would be difficult to predict how the compositions influence the final crystal behavior in terms of performance (e.g., as detecting devices). The direction of the g jitter is assumed to be the same as that of the residual gravity vector, i.e., oriented normally to the ampoule. The upper- and lower-side boundaries are presumed to be adiabatic. Translation of the ampoule is taken into account by supplying a doped melt of dilute bulk composition at a constant velocity (growth velocity) at the left of the computational space (feed zone) and withdrawing a solid of composition $c_s = c_s(x, t)$ from the right (crystal–melt interface). The interface is located at a distance from the feed zone, and its temperature is supposed to be uniform and constant with time and equal to the melting temperature of the crystal. Because we wish to confine our attention to the concentration distortions caused by thermal buoyancy and vibrational convection, rather than to variations resulting from nonplanar crystal–melt interfaces, the interface is supposed to be flat in our model. The left boundary is at a higher temperature.

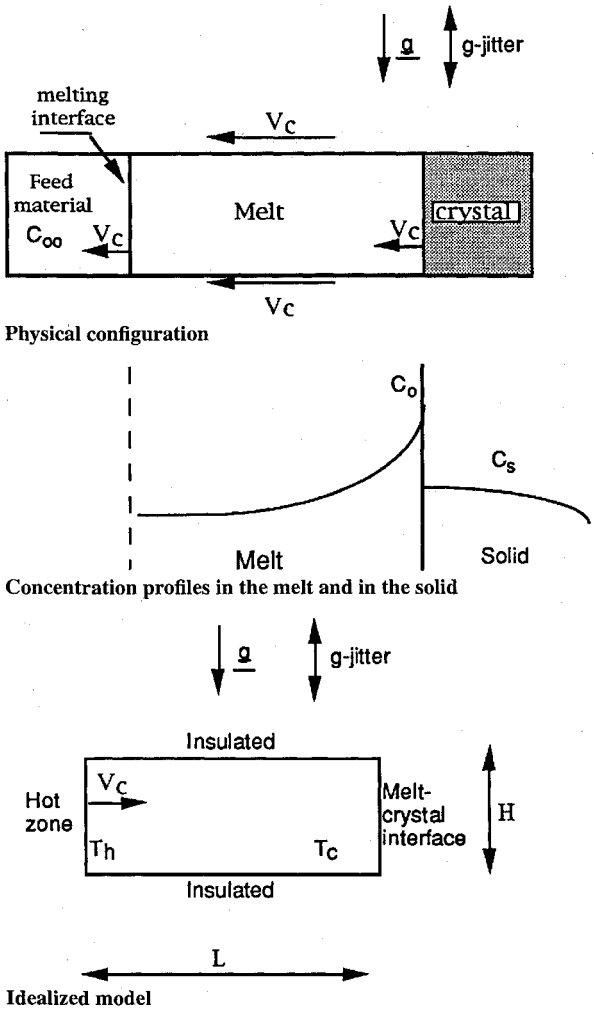

Fig. 4 Geometry of the problem.

The governing equations were written in nondimensional form using L, α/L, $\rho\alpha^2/L^2$, $T_h - T_c$, and c_∞ to scale the lengths, velocity, pressure, temperature, and solute concentration. The initial conditions are

$$t = 0, \quad \text{for} \quad 0 < x < 1 \quad \text{and} \quad 0 < y < 0.5$$

$$u(x, y) = Pe_c\, Pr/Sc \tag{18a}$$

$$v(x, y) = 0 \tag{18b}$$

$$T(x, y) = 1 \tag{18c}$$

$$c(x, y) = 0 \tag{18d}$$

As boundary conditions, we assumed that
on the crystal-melt interface ($0 \le y \le 0.5$)

$$T(1, y) = 0 \tag{19a}$$

$$u(1, y) = Pe_c \cdot Pr/Sc \cdot \sigma \tag{19b}$$

$$v(1, y) = 0 \tag{19c}$$

$$c_x(1, y) = Pe_c \cdot (1 - k) \cdot c(1, y) \tag{19d}$$

on the feed zone ($0 \le y \le 0.5$)

$$T(0, y) = 1 \tag{20a}$$

$$u(0, y) = Pe_c \cdot Pr/Sc \tag{20b}$$

$$v(0, y) = 0 \tag{20c}$$

$$c_x(0, y) = Pe_c \cdot [c(0, y) - 1] \tag{20d}$$

on the insulated boundaries ($0 \le x \le 1$)

$$T_y(x, y = 0; y = 0.5) = 0 \tag{21a}$$

$$u(x, y = 0; y = 0.5) = 0 \tag{21b}$$

$$v(x, y = 0; y = 0.5) = 0 \tag{21c}$$

$$c_y(x, y = 0; y = 0.5) = 0 \tag{21d}$$

For the vector field w, homogeneous initial and boundary conditions are imposed.

The problem was solved numerically with the numerical method of control volumes by a modified MAC (marker and cell) method explicit in time. The domain was discretized with a staggered grid and the field equations, in the primitive variables (u, v, p), were numerically integrated using a classic second-order central-difference scheme for the diffusive terms and a quadratic-interpolation upwind method for the convective terms. A preliminary independent verification of the numerical procedure has been carried out to validate the code and to select a mesh size sufficient for the calculations. When the number of grid points was increased, a converging behavior was found; in particular, for the parametrical analysis described in the next section, we used a mesh of 40 × 20 grid points, for which an error less than 3% was found when compared with finer meshes.

Results and Discussion

In the numerical calculations, the following geometric parameters have been considered: $L = 1$ [cm] and $H = 0.5$ [cm]. The temperature difference was $\Delta T = 200$ [K]. As the fluid, we considered gallium-doped germanium, with the following properties:

$$\alpha = 0.1\,[\mathrm{cm}^2/\mathrm{s}], \qquad \nu = 10^{-3}[\mathrm{cm}^2/\mathrm{s}]$$

$$D = 2.5 \times 10^{-5}[\mathrm{cm}^2/\mathrm{s}], \qquad \beta_T = 2.5 \times 10^{-4}\mathrm{K}^{-1}$$

$$Pr = 10^{-2}, \quad Sc = 40, \quad Pe_c = 2, \quad k = 0.1, \quad \sigma = 1$$

For this case there is the following dependence of the gravitational Peclet number on the residual-gravity level:

$$Pe_g \approx 5 \times 10^5 G_s$$

The numerical results are presented and discussed in terms of streamlines, velocity fields, isoconcentrations, and concentration profiles. The solute distortions, i.e., the differences of the concentration field, in the presence of residual gravity and g jitter, with respect to the ideal zero-gravity field, are reported as functions of the Peclet number (Pe_g), for steady g, and of the vibrational Peclet number (Pe_v), for high-frequency g jitter. Because of the small value of the Prandtl number, the temperature field is relatively insensitive to convection and is characterized by a linear distribution along the horizontal adiabatic walls.

In Figs. 5–7, the streamlines, the computed velocity fields, and the corresponding concentration distributions are shown at steady state for $Pe_v = 0$ (no g jitter) and different gravitational Peclet numbers ($Pe_g = 0, 0.05, 0.5$) corresponding, respectively, to zero-gravity and residual-gravity levels $G_s = 10^{-7}, 10^{-6}$. In zero-gravity, the velocity vectors (Fig. 5b) are directed from the feed to the crystal, are equal to the crystal growth velocity v_c, and are oriented normally

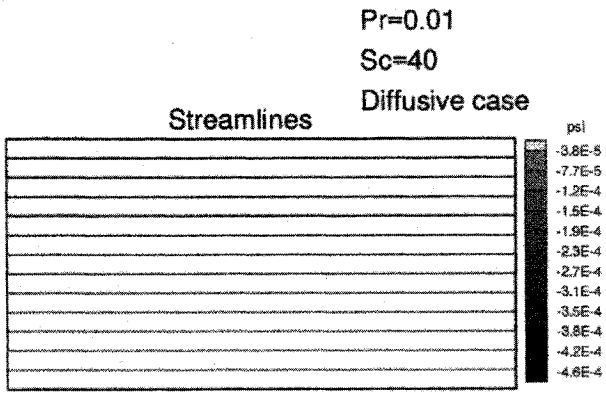

a) Streamlines

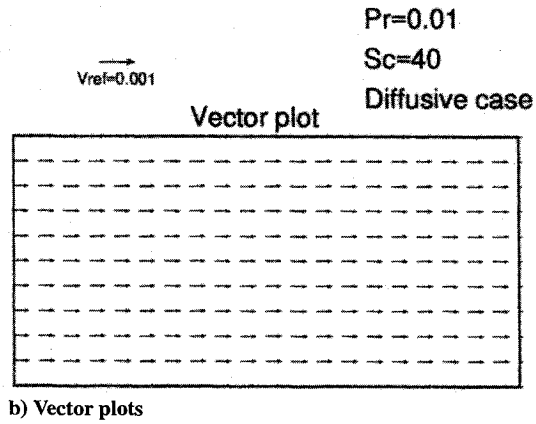

b) Vector plots

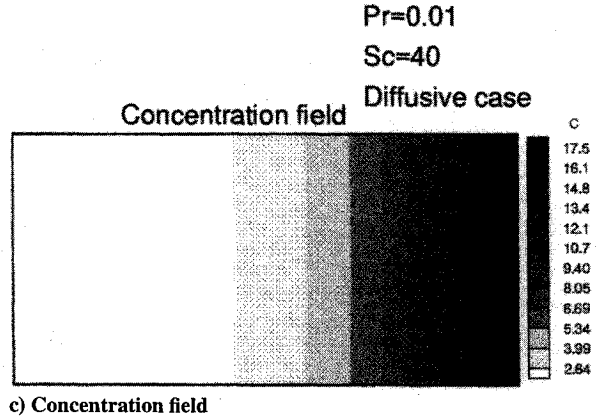

c) Concentration field

Fig. 5 Streamlines, vector plots, and concentration field for zero gravity ($Pe_g = 0$ and $Pe_v = 0$).

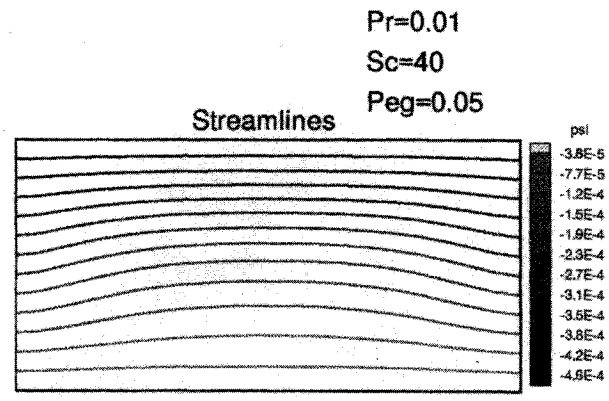

a) Streamlines

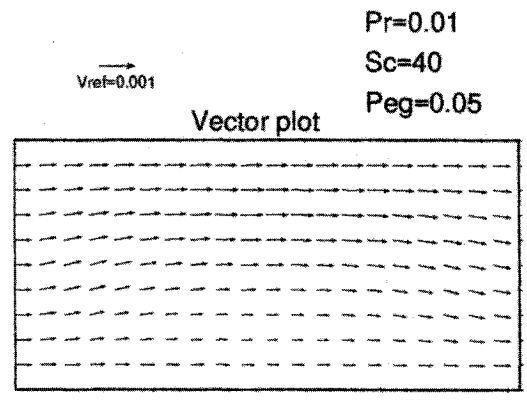

b) Vector plots

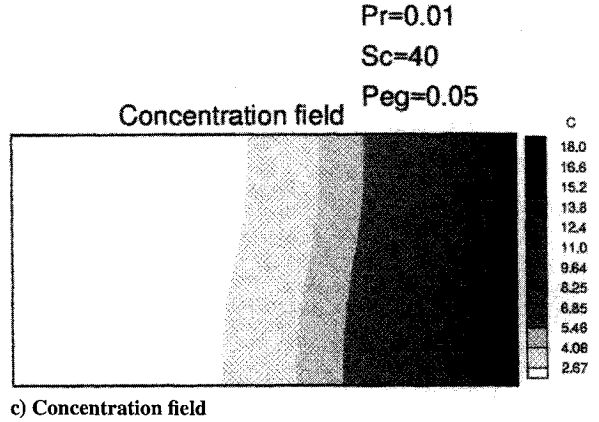

c) Concentration field

Fig. 6 Streamlines, vector plots, and concentration field for residual gravity, without any g jitter: $Pe_g = 0.05$ and $Pe_v = 0$.

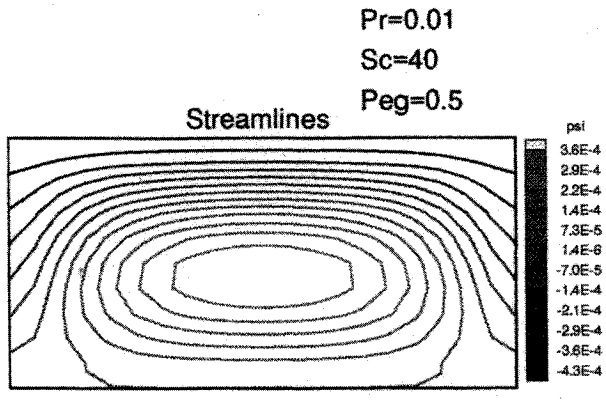

a) Streamlines

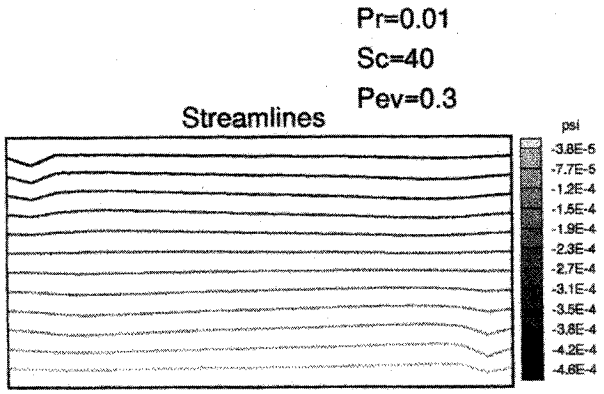

a) Streamlines

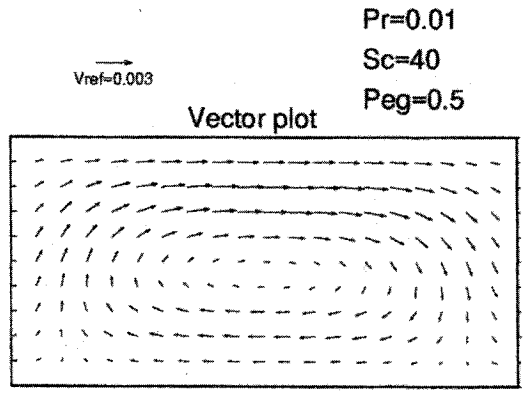

b) Vector plots

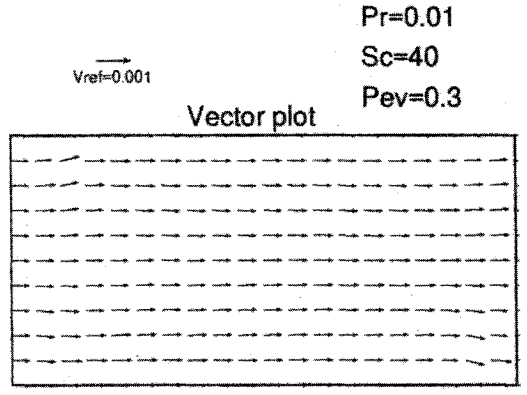

b) Vector plots

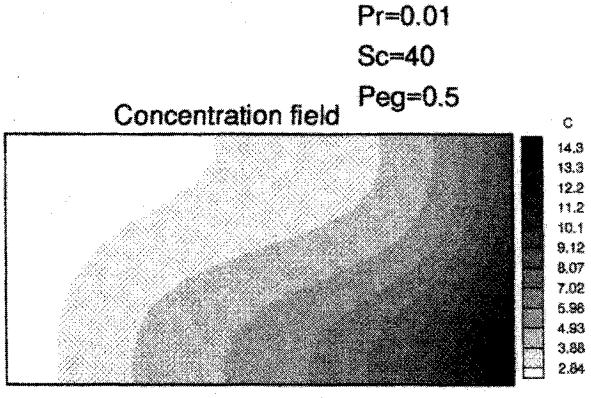

c) Concentration field

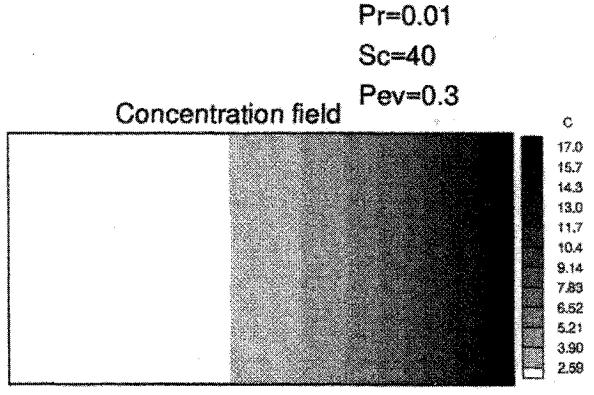

c) Concentration field

Fig. 7 Streamlines, vector plots, and concentration field for residual gravity, without any *g* jitter: $Pe_g = 0.5$ and $Pe_v = 0$.

Fig. 8 Streamlines, vector plots, and concentration field for *g* jitter, without any residual gravity: $Pe_v = 0.3$ and $Pe_g = 0$.

to the crystal–melt interface. The isoconcentration lines are parallel to the interface (Fig. 5c). For low Pe_g numbers, the buoyancy forces, resulting from residual-gravity acceleration, deform the velocity field upward, resulting in the appearance of a weak vortex cell rotating clockwise. When Pe_g increases, the intensity of the flow increases (Fig. 7). As a consequence, the isoconcentrations are strongly deformed as compared with the diffusive situation.

Figures 8–10 show the streamlines, the vector plots, and the corresponding concentration distributions in the absence of residual-gravity levels ($Pe_g = 0$) for three different values of the vibrational Peclet number ($Pe_v = 0.3, 3, 30$) corresponding to *g* jitter of amplitudes in the range $G = 10^{-3}$–10^{-2} at frequencies of about 1 Hz. For low Pe_v numbers, we can see a little distortion of the velocity field in the corner regions of the ampoule. When the Pe_v number increases, the vibrational forces become more important and a steady regime with a symmetric four-cell structure is obtained. In this situation, relevant distortions of the averaged concentration profiles are present. This concentration distortion in the melt is expected to persist in the crystal after solidification.

The characterization of melt-grown crystals often includes radially or laterally averaged longitudinal composition profiles. Longitudinal concentration profiles are shown in Fig. 11a for different residual accelerations. The purely diffusive case is represented by the dashed line. For $Pe_g = 0.5$ ($G_s = 10^{-6}$), the concentration profile is significantly distorted when compared with the ideal diffusive one, and the distortion is even larger for $Pe_g = 5$ ($G_s = 10^{-5}$). The corresponding interface concentration profiles, related to the lateral variation in composition of the crystal, are illustrated in Fig. 11b. When the residual acceleration increases, the buoyancy-driven recirculation dominates; the longitudinal concentration gradient is reduced (Fig. 11a), and the lateral concentration gradient along the interface increases (Fig. 11b).

To quantify the differences between the concentration profiles in the presence of residual accelerations and the ideal zero-gravity

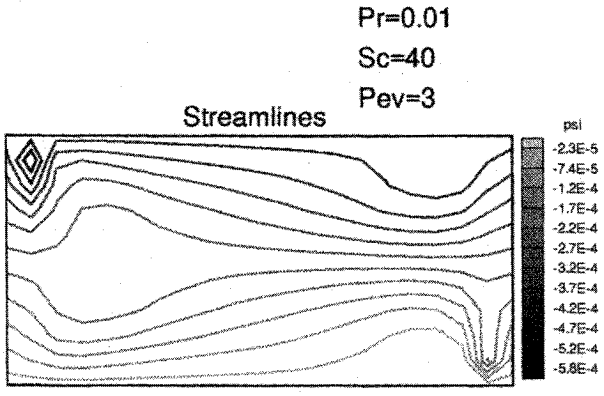

a) Streamlines

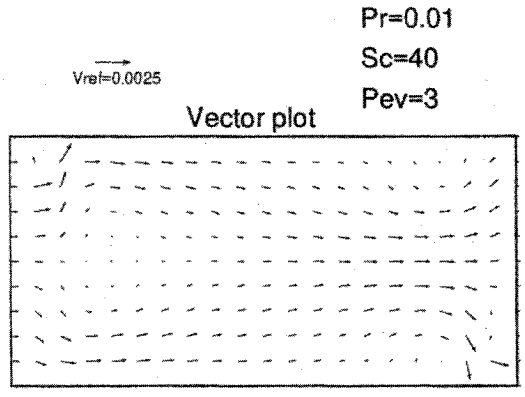

b) Vector plots

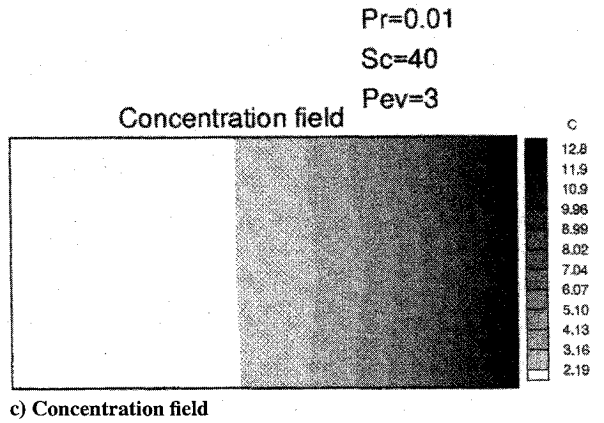

c) Concentration field

Fig. 9 Streamlines, vector plots, and concentration field for g jitter, without any residual gravity: $Pe_v = 3$ and $Pe_g = 0$.

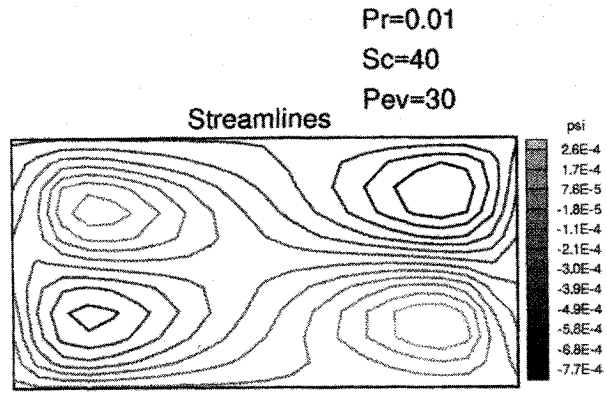

a) Streamlines

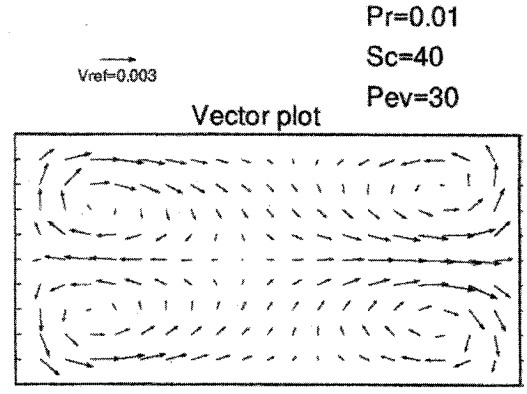

b) Vector plots

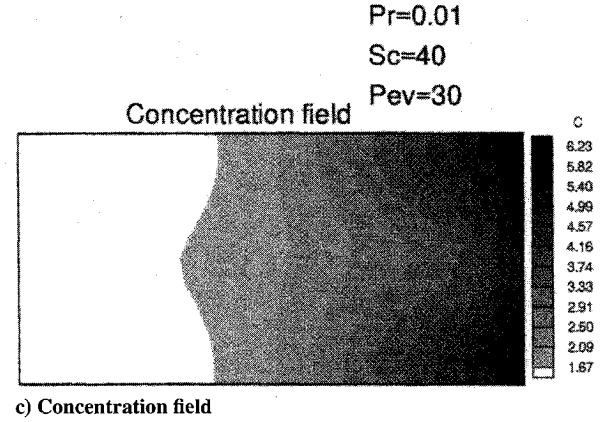

c) Concentration field

Fig. 10 Streamlines, vector plots, and concentration field for g jitter, without any residual gravity: $Pe_v = 30$ and $Pe_g = 0$.

profiles, we introduced a radial and a longitudinal solute distortion, defined by

$$\varepsilon_{\text{rad}} = \frac{c_{\max}(1) - c_{\min}(1)}{c_{\text{med}}(1)}$$

$$\varepsilon_{\text{long}} = \frac{c_{\text{diff}}(1) - c(1)}{c_{\text{med}}(1)}$$

where the subscripts max, min, and med denote the maximum, minimum, and average concentrations, respectively. The earlier distortions are plotted as functions of Pe_g (Fig. 11c). They are monotonically increasing functions of the Peclet number but, in the range of interest, the radial distortion is higher than the longitudinal one.

The computational modeling of the distribution of solute for steady acceleration normal to the density gradient has been treated by Alexander et al.,[10] who considered a different configuration and somewhat different values of the growth parameters (in their system, the top and bottom walls include isothermal zones and a thermal barrier that is modeled using adiabatic conditions). For $G = 10^{-6}$, those authors found a relative distortion in the composition of the melt at interface equal to 0.11, whereas in the present case, $\varepsilon_{\max} = 0.48$. According to Garandet,[16] the relative radial segregation should scale as a function of Pe_c and of the product $Re_g Sc$. Because of the different physical parameters considered, the product $Re_g Sc$ is 148 in Ref. 10 and 2×10^3 in the present case. Therefore, the computed distortions are not inconsistent with the results reported by Alexander et al.,[10] because in the present case, the product is one order of magnitude larger. For $G = 10^{-7}$, $Re_g Sc = 200$, and we found $\varepsilon_{\max} = 0.1$, which is very close to the maximum distortion computed by Alexander et al.[10] for a value of $Re_g Sc$ of the same order of magnitude ($Re_g Sc = 148$). We stress, however, that a direct comparison between the present calculations and the results obtained by Alexander et al.[10] cannot be performed because of the different value of Pe_c and the different thermal boundary conditions.

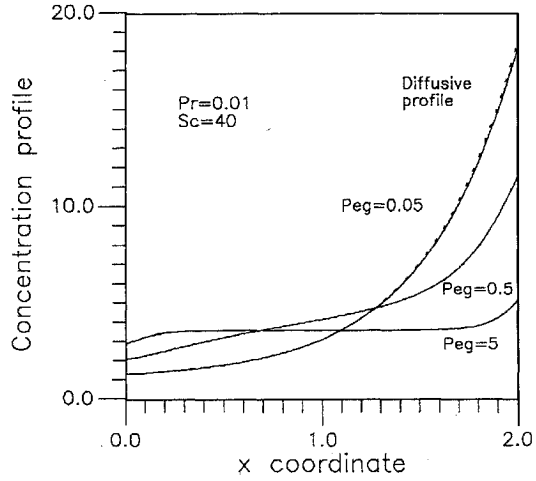

a) Concentration profiles along the x coordinate for $y = 0.25$, for different gravitational Peclet numbers Pe_g

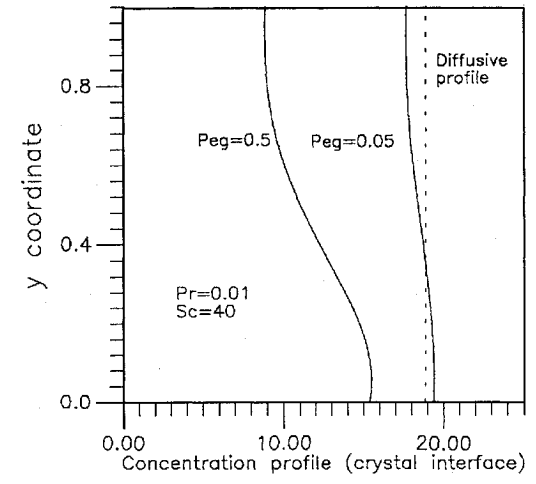

b) Concentration profiles at the crystal-melt interface, for different gravitational Peclet numbers

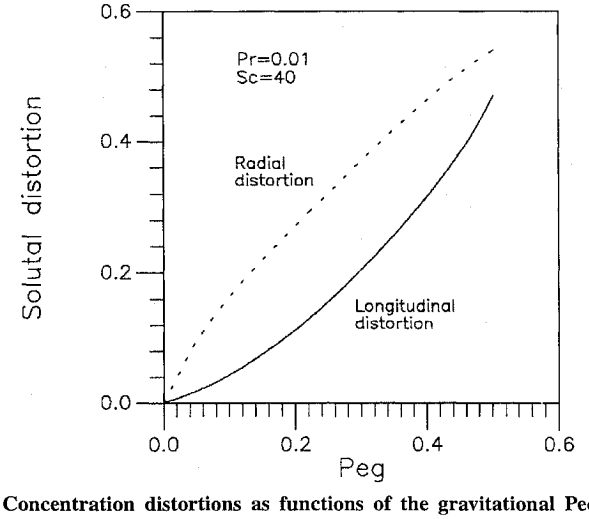

c) Concentration distortions as functions of the gravitational Peclet number

Fig. 11 Concentration profiles and distortions for steady natural convection ($Pe_v = 0$).

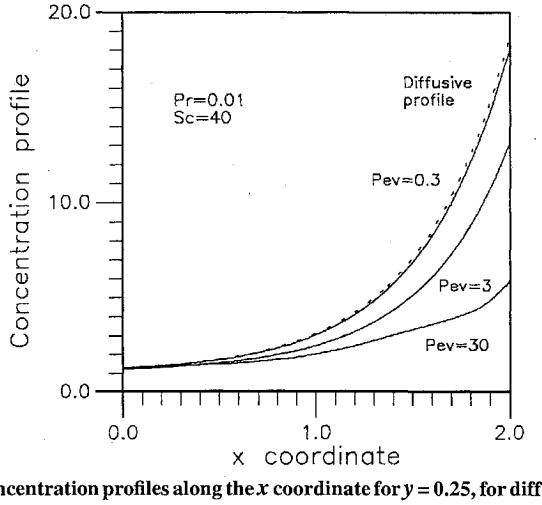

a) Concentration profiles along the x coordinate for $y = 0.25$, for different vibrational Peclet numbers

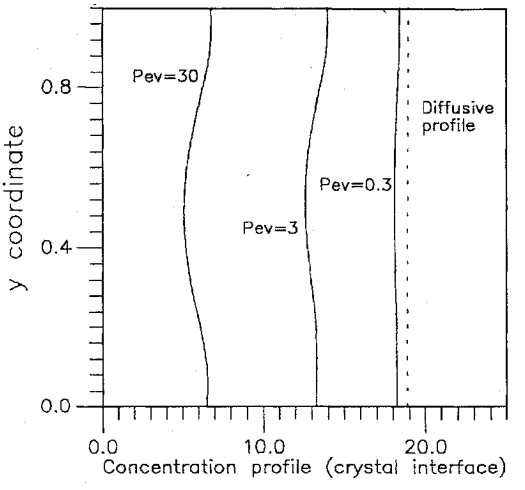

b) Concentration profiles at the crystal-melt interface, for different vibrational Peclet numbers

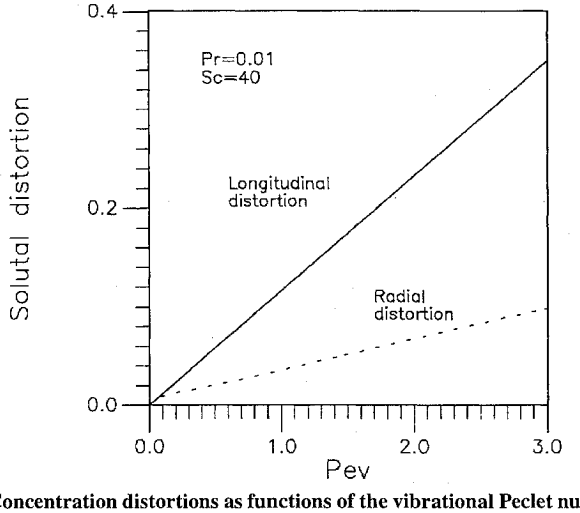

c) Concentration distortions as functions of the vibrational Peclet number

Fig. 12 Concentration profiles and distortions for time-averaged vibrational convection ($Pe_g = 0$).

In Fig. 12, the longitudinal (Fig. 12a) and interface (Fig. 12b) concentration profiles are shown in the case of g jitter, for different vibrational Peclet numbers. The corresponding radial and longitudinal distortions are illustrated in Fig. 12c.

The main difference compared to the case of steady gravity is that the radial distortion is smaller than the longitudinal one. This result is explained by the different flowfield organizations, in the cases of natural and vibrational convection. In the first case (buoyancy-driven convection), there is a single elongated vortex cell in the ampoule with melt flowing down in the region near the crystal–melt interface. The velocity is directed toward the crystal in the upper half of the interface and from the crystal to the melt in the lower one, causing large deformations of the interface profile. In the second case (vibrational convection), the flow structure is characterized by two pairs of vortex cells located near the left and the right sides of the ampoule. The two counterrotating vortices near the crystal are

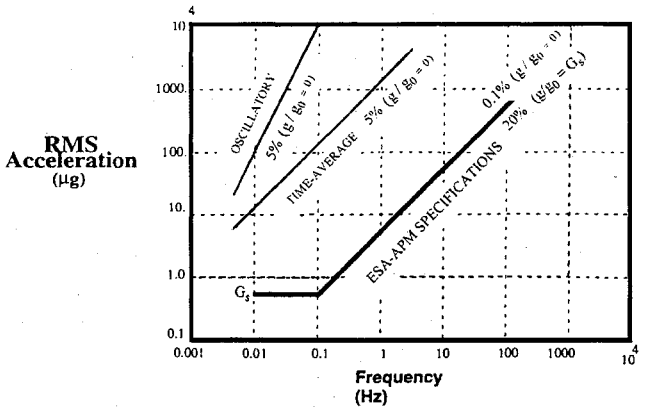

Fig. 13 Tolerability limits in the plane (frequency, acceleration).

responsible for smaller average deformations of the concentration profile.

Alexander et al.[11] carried out numerical computations of high-frequency vibration on Bridgman growth systems. For a sinusoidal acceleration of frequency $f = 1$ [Hz] and amplitude $G = 10^{-2}$, they found that the velocity field oscillated back and forth in large convective rolls, with a steady-state compositional variation, suggesting the presence of nonzero time-averaged flows. In particular, for $Sc = 50$, they computed a time-averaged composition nonuniformity $\varepsilon_{\max} = 0.16$, which is not inconsistent with the present calculations, which give, for $Pe_v = 3$ (G between 10^{-3} and 10^{-2}) and $Sc = 40$, a maximum concentration distortion $\varepsilon_{\max} = 0.1$.

In correspondence to a maximum allowable radial distortion of 5%, the tolerability curves obtained theoretically from the scaling analysis have been particularized and compared with the European Space Agency–Attached Pressurized Module (ESA–APM) specifications (Fig. 13). The tolerability domains as measured by acceleration as a function of frequency, show that the limits associated with time-averaged distortions are always more stringent when compared with those corresponding to oscillatory distortions induced by single-frequency periodic accelerations. However, in the absence of any residual gravity, these limits are higher than the ESA specifications, corresponding to a radial distortion of about 0.1%. In presence of a residual-gravity level $G_s = 7 \times 10^{-7}$, the computed radial distortion is about 20%. Therefore, we conclude that, unlike other microgravity processes, such as experiments for the measurement of diffusion coefficients, in this case the ESA specifications could be appropriate in the absence of any residual-gravity level, but relevant distortions may be induced by residual-gravity effects.

Conclusions

In this study, we investigate the effects of residual gravity and g jitter on typical fluid dynamic and material science experiments, to extend the tolerability limits obtained with previous scaling analyses (accounting only for oscillatory distortions induced by single-frequency periodic g jitter) to the more general case of oscillatory and time-averaged distortions related to nonlinear vibrational effects.

As a study case, a typical Bridgman crystal-growth experiment is considered. The model allows computation of radial and longitudinal distortions of the concentration profiles in the melt, although it is difficult to extrapolate these distortions to the final quality of the crystals. As in previous works, however, the concentration distortions in the melt could be assumed to induce similar distortions also in the solid.

The numerical computations show that the tolerability limits associated with time-averaged distortions are more stringent than those corresponding to oscillatory distortions. The comparison between the numerically computed tolerability curves and the ESA–APM specifications show that, in this particular case, the ESA specifications could be appropriate in the absence of any residual gravity, but relevant distortions may be induced by residual-gravity effects. However, we must underline that this conclusion is based on a model with a number of simplifications (e.g., flat solid–liquid interface, two-dimensional flow, residual acceleration oriented normally to the ampoule axis) and may not accurately reflect all of the conditions that occur in the actual growth of semiconductors in space. In particular, we believe that the effects of interface curvature and of the three-dimensionality of the flow, caused by the variation of the acceleration orientation, should be addressed in future works.

Furthermore, the present analysis has been focused on the effects of steady residual and of high-frequency sinusoidal accelerations. The most common disturbances on board space platforms are those produced by impulsive transients (e. g., pulselike acceleration resulting from crew operation of the onboard equipment, to firing activity) that induce oscillations at the natural frequency and that decay after a while (a few cycles). Further assessment must be developed to evaluate, in these cases, the minimum number of cycles sufficient to generate time-averaged distortions and the limits of validity of the time-averaged models for the evaluation of these distortions.

Acknowledgment

This work was supported by the European Space Agency under Contract 22054/94/ F/FL.

References

[1]Knabe, W., and Eilers, D., "Low-Gravity Environment in Spacelab," *Astronautica Acta*, Vol. 9, No. 4, 1982, pp. 187–198.

[2]Hamacher, H., Fitton, B., and Kingdom, J., "The Environment of Earth-Orbiting Systems," *Fluid Sciences and Material Sciences in Space*, edited by H.U. Walter, Springer–Verlag, Berlin, 1987, pp. 1–50.

[3]Rogers, M. J. B., and DeLombard, R., "Summary Report of Mission Acceleration Measurements for STS-65," NASA TM-106871, March 1995.

[4]Monti, R., Langbein, D., and Favier, J. J., "Influence of Residual Accelerations on Fluid Physics and Material Science Experiments," *Fluid Sciences and Material Sciences in Space*, edited by H. U. Walter, Springer–Verlag, Berlin, 1987, pp. 637–680.

[5]Camel, D., and Favier, J. J., "Scaling Analysis of Convective Solute Transport and Segregation in Bridgman Crystal Growth from the Doped Melt," *Journal de Physique (Paris)*, Vol. 46, No. 6, 1986, pp. 1001–1014.

[6]Alexander, J., and Rosenberger, F., "Bridgman Crystal Growth in Low Gravity: A Scaling Analysis," *Low-Gravity Fluid Dynamics and Transport Phenomena*, edited by J. N. Koster and R. L. Sani, Vol. 130, Progress in Astronautics and Aeronautics, AIAA, Washington, DC, 1990, pp. 87–117.

[7]Thevenard, D., and Ben Hadid, H., "Low Prandtl Number Convection in a Rectangular Cavity with Longitudinal Thermal Gradient and Transverse g-Jitters," *International Journal of Heat and Mass Transfer*, Vol. 34, No. 8, 1991, pp. 2167–2173.

[8]Jue, T. C., and Ramaswamy, B., "Natural Convection with Thermocapillary and Gravity Modulation Effects in Low-Gravity Environments," *Journal of Spacecraft and Rockets*, Vol. 29, No. 6, 1992, pp. 856–869.

[9]Kamotani, Y., Prasad, A., and Ostrach, S., "Thermal Convection in an Enclosure Due to Vibrations Aboard a Spacecraft," *AIAA Journal*, Vol. 19, No. 4, 1981, pp. 511–516.

[10]Alexander, J. I., Ouazzani, J., and Rosenberger, F., "Analysis of the Low Gravity Tolerance of Bridgman–Stockbarger Crystal Growth I. Steady and Impulse Accelerations," *Journal of Crystal Growth*, Vol. 97, No. 2 , 1989, pp. 285–302.

[11]Alexander, J. I., Amiroudine, S., Ouazzani, J., and Rosenberger, F., "Analysis of the Low Gravity Tolerance of Bridgman–Stockbarger Crystal Growth II. Transient and Periodic Accelerations." *Journal of Crystal Growth*, Vol. 113, No. 1, 1991, pp. 21–38.

[12]Alexander, J. I., "Estimation of Experiment Sensitivity to Residual Acceleration," *Microgravity Quarterly*, Vol. 5, No. 1, 1995 pp. 23–28.

[13]Gershuni, G. Z., Zhukhovitskii, E. M., and Yurkov, Yu. S., "Vibrational Thermal Convection in a Rectangular Cavity," *Fluid Dynamics*, Vol. 17, No. 4, 1982, pp. 94–99

[14]Chenrnatynski, V. I., Gershuni, G. Z., Monti, R., and Savino, R., "Transient Effects of g-Pulses in a Fluid Cell Heated from Below," *Microgravity Quarterly*, Vol. 5, No. 3, 1995, pp. 152–161 .

[15]Monti, R., and Savino, R., "The Basis and the Recent Developments of Napolitano's Scaling and Order of Magnitude Analysis." *Microgravity Quarterly*, Vol. 5, No. 1, 1995, pp. 13–18.

[16]Garandet, J. P., "On the Relevance of Scaling Analyses for Solute Transport Problems," *Microgravity Quarterly*, Vol. 5, No. 1, 1995, pp. 19–22.

I. E. Vas
Associate Editor